

TROPOSPHERIC WATER VAPOR OBSERVATIONS USING A RAMAN LIDAR OVER HEFEI*

WU Yonghua (吴永华), HU Huanling (胡欢陵), HU Shunxing (胡顺星),

LI Chen (李琛) and ZHOU Jun (周军)

Anhui Institute of Optics and Fine Mechanics, Chinese Academy of Sciences, Hefei 230031

Received May 21, 2003; revised September 20, 2003

ABSTRACT

This paper presents a Raman lidar for measuring tropospheric water vapor profiles over Hefei (31.9°N, 117.17°E), China. Intercomparisons of water vapor mixing ratio obtained by this Raman lidar and GZZ-59 type radiosonde observations show the good agreements when relative humidity is higher than 20%. Typical vertical profiles and seasonal variations of water vapor mixing ratio distribution are reported. Many observation cases indicate that the high moisture layer corresponds to large aerosol scattering ratios in the lower troposphere.

Key words: water vapor, troposphere, Raman scattering, lidar

1. INTRODUCTION

Water vapor (H_2O) is one of the active and key atmospheric traces. It has strong absorption effects in the infrared (IR) and microwave bands of solar-earth radiation. Meantime, it is crucial in the precipitation and cloud formation. Therefore, water vapor distribution plays an important role in meteorology, atmospheric radiation and climate change (Shine and Sinda 1991). Currently, passive ground-based or space-based microwave radiometers and IR spectrometers can measure the column content of water vapor in the atmosphere, they also can retrieve water vapor distribution profile with lower spatial resolution. Radiosonde can make the routine measurements of moisture twice a day in the meteorological stations, but the sensitivity and accuracy of humidity sensor limit its measuring precision and maximum altitude (Zhang and Zhao 2000). Lidar (Light Detection Range) applications in atmospheric remote sensing become wider and wider due to its higher spatial and temporal resolution. Raman lidar is a good candidate for measuring tropospheric water vapor profiles, and its potential capacity has been demonstrated and validated (Whiteman et al. 1992; Ferrare et al. 1995; Wessel et al. 2000). Meantime, Raman lidar also can get the aerosol optical parameters with higher accuracy algorithm, moreover its whole system is not same complicated as differential absorption lidar (Grant 1991). Therefore in recent years, Raman lidar has advanced water vapor and aerosol observations, and it has been deployed for the continuous and autonomous measurements of water vapor and aerosol in many field campaigns (Melfi et

* Supported by the National 863 High Technology Research and Development Project.

al. 1995, Turner et al. 2000). This paper describes a Raman lidar for the measurements of tropospheric water vapor in the nighttime over Hefei (31.9°N, 117.17°E), China, some typical vertical profiles of water vapor distribution are presented.

II. L625 RAMAN LIDAR AND MEASURING PRINCIPLE

L625 Raman lidar is briefly overviewed here. It operates with the frequency-tripled Nd:YAG laser at 355 nm, whose pulse energies are about 60 mJ with repetition rates of 10 Hz. Raman scattering returns of water vapor, nitrogen and elastic scattering are simultaneously collected by a 62.5 cm diameter Cassegrain telescope. Based on the previous system (Li et al. 2000), optical receiving units are improved so that this lidar can quasi-simultaneously measure the distribution of ozone, aerosol and water vapor. A fused silica optical fiber and its couplers guide these light signals into beam-splitter unit. This fiber has 2 mm core diameter and numerical aperture 0.36, which fits with field of view 2 mrad for the receiving optical system. Transmission of fiber is larger than 95% per meter over the wavelength range of 355 nm to 532 nm. Fiber coupler and collimators are designed with all of reflecting mirrors in order to overcoming dichromatic effects of different wavelengths. Three layers of beam-splitters are designed for water vapor, ozone and aerosol measurement, respectively. Backscattering light signals are detected by three cooled photomultipliers (PMT) for H₂O-Raman (407.4 nm), N₂-Raman (386.7 nm) and elastic scattering (355 nm), respectively. Thoron EMI PMTs operate with a temperature -20°C for reducing thermal and dark current noises. Interference filters placed in front of PMTs are the key components for rejecting the cross-talk of elastic scattering (Mie-Rayleigh) returns in H₂O-Raman and N₂-Raman channels. Both of them have the block ratio 10⁻¹² at wavelength 355 nm and 532 nm. For Raman channels, the transmission values of filter are about 55% at 407.4 nm and 60% at 386.7 nm, respectively. Filter bandwidth with 4.7 nm is considered to overcome the variation of Raman scattering cross-section with different temperature (Whiteman et al. 1993). In elastic scattering channel, bandpass of interference filter is 1 nm with block ratio 10⁻⁵ for background radiation noise. Outputs of PMTs are firstly amplified by the fast preamplifiers, then checked by three multi-channel scalers (EG&G T914P) with maximum counting rate 150 MHz. Considering the saturation and nonlinear effects of detectors or scalers caused by overstrong signals from lower altitudes, neutral density filters are usually added in N₂-Raman and elastic scattering channels. Because of uncoaxiality of optical transmitter and receiver, this lidar can receive the useful signals above 0.6 km altitude.

Water vapor mixing ratios can be derived from the ratios of H₂O-Raman to N₂-Raman scattering signals in the following formula (Whiteman et al. 1992):

$$W(z) = K \frac{p(\lambda_{\text{H}_2\text{O}}, z) q(\lambda_{\text{H}_2\text{O}}, \lambda_0, z)}{p(\lambda_{\text{N}_2}, z) q(\lambda_{\text{N}_2}, \lambda_0, z)}, \quad (1)$$

where $W(z)$ is water vapor mixing ratio, K is the ratio of optical constants between H₂O-Raman channel and N₂-Raman channel, which is related to the transmission of optical receiver and the quantum efficiency of detector. $\lambda_{\text{H}_2\text{O}}$, λ_{N_2} and λ_0 are H₂O-Raman shift wavelength, N₂-Raman shift wavelength and laser wavelength, respectively. $P(\lambda_{\text{H}_2\text{O}}, z)$ and $P(\lambda_{\text{N}_2}, z)$ are H₂O-Raman signal and N₂-Raman signal, respectively. $q(\lambda_{\text{H}_2\text{O}}, \lambda_0, z)$ and

$q(\lambda_N, \lambda_0, z)$ correspond to atmospheric transmission for H₂O-Raman and N₂-Raman scattering signals.

Systematic constant ratio K in Formula (1) is calibrated by best-fitting lidar signal ratios with the moisture of radiosonde (Whiteman et al. 1993; Ferrare et al. 1995). We get the mean value of K by combining one-week long or more measurements of radiosonde. Routine radiosonde observations have been made twice a day over Hefei, so we can periodically check the variability of calibration constant. Mean value of K will be used if there is no radiosonde data during Raman lidar observations. From the equation above, water vapor mixing ratios are proportional to the ratios of H₂O-Raman to N₂-Raman scattering signals, they are not sensitive to the geometric overlap factors between laser beam and field of view of optical receiver in every Raman channel. We also add N₂-Raman filter in H₂O-Raman channel to correct the slight differences of optical alignment between H₂O-Raman and N₂-Raman channel. Because difference of H₂O-Raman and N₂-Raman shift wavelength is not large, their transmission ratios are usually a few percent below 10 km altitude in the cloudless night. Systematic errors caused transmission ratios of H₂O-Raman to N₂-Raman channel are reduced by correcting aerosol attenuation derived by N₂-Raman and elastic scattering signals (Wu et al. 2002). Currently, L625 Raman lidar makes the regular nighttime measurements of water vapor at Hefei. One signal profile is recorded with integrated laser shots 5000 and spatial resolution 30 m. In order to reduce the statistic errors caused by photon-count fluctuations and noises, water vapor mixing ratio distributions are derived by integrating the returns of laser shots 40000, and the raw signals are running-smoothed with range of 210 m below 2.5 km altitude and 300–600 m above 2.5 km altitude.

III. MEASUREMENT RESULTS AND DISCUSSIONS

Figure 1 shows water vapor mixing ratio distribution obtained by L625 Raman lidar and GZZ-59 type radiosonde over Hefei. Short bars represent the statistic errors of water vapor measured by L625 Raman lidar, thin solid line represents water vapor mixing ratios corresponding to 20% relative humidity (RH). Figure 1a gives water vapor profiles in the nighttime of September 22, 2000. Statistic errors of Raman lidar measurement are usually less than 5% below 4.5 km altitude, less than 15% between 4.5 km and 9 km altitudes. Water vapor profile of Raman lidar agrees well with the radiosonde data. Generally, their discrepancies are less than 20% except the altitude range of 4.0 km to 5.5 km, where relative humidity are less than 20%. Figure 1b presents another example of water vapor mixing ratios obtained by Raman lidar and radiosonde on April 1, 2001. They are consistent with each other between 0.6 km and 6 km altitudes. But lidar results are drier than the radiosonde results between 2 km and 4.5 km altitudes where relative humidities are not higher than 20%. Figure 1c illustrates the profiles of water vapor mixing ratios observed by L625 Raman lidar and radiosonde on August 23, 2002, they agree well with each other from 1.5 km to 9.5 km altitude. Below 1.5 km altitude, large differences are probably caused by the slight saturation of N₂-Raman signals. Figure 1d shows the consistent water vapor mixing ratio distributions obtained by L625 Raman lidar and GZZ-59 type radiosonde on June 6, 2002.

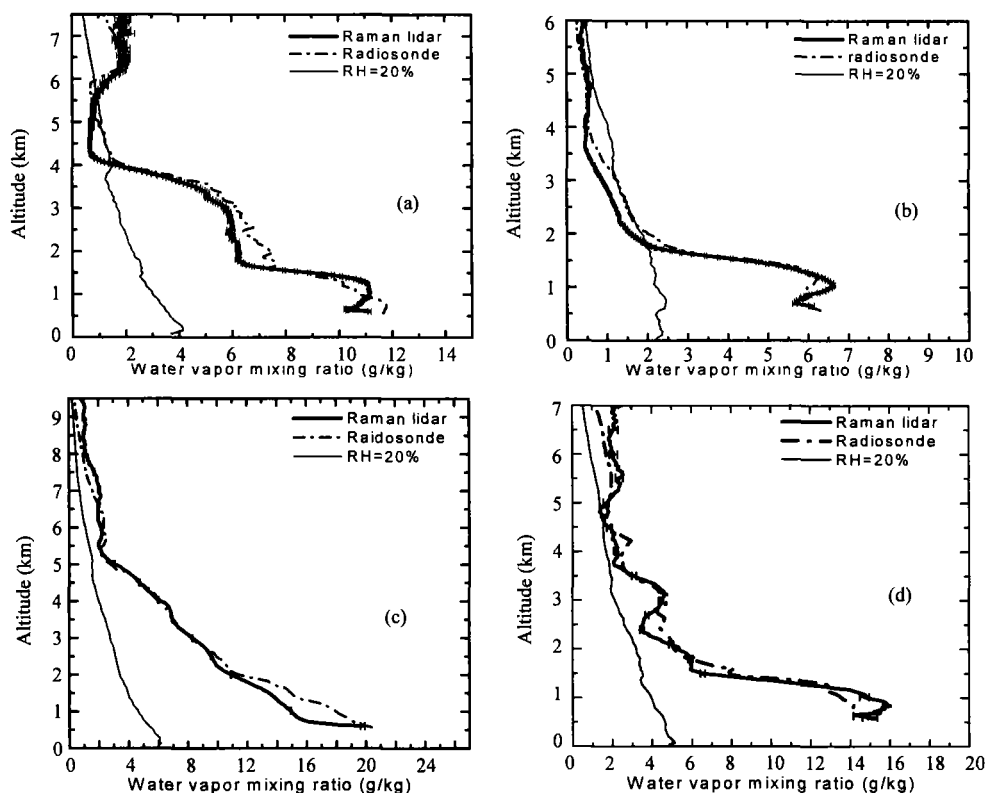


Fig. 1. Water vapor mixing ratio distributions measured by L625 Raman lidar and GZZ-59 radiosonde on (a) September 22, 2000, (b) April 1, 2001, (c) August 23, 2002 and (d) June 6, 2002.

Water vapor measurements by L625 Raman lidar usually attain 6 km altitude in spring and winter due to lower moisture in these two seasons. But in summertime, this Raman lidar measurement can attain higher altitudes because of higher moisture. General distribution characteristics of water vapor are drawn from Fig. 1, rich water vapor mainly exists below 3 km altitude over Hefei, but other moisture layer sometimes can be found above 3 km altitude. Sharp gradients of water vapor distribution appear between 1.0 km and 2.0 km altitude, which are correlated to the thermal and dynamic process in the planetary boundary layer.

Figure 2 illustrates the mean differences of water vapor mixing ratios between Raman lidar and GZZ-59 radiosonde 17 nighttime observations during 2001–2002. It can be seen that their mean differences are usually less than 20%, but become larger between 2 km and 5 km altitude, where lidar results are lower than ones of radiosonde, which probably result from large errors of GZZ-59 radiosonde observations in the dry and sharp moisture gradient layer. By comparing with RS-80 and VIZ-1392 radiosonde, the systematic bias of GZZ-59 radiosonde measuring moisture is usually between 5% and 10% under the warm and moderate moisture conditions, but worse at the temperature below 0°C or in lower moisture air ($RH < 20\%$) (Zhang and Zhao 2000). Intercomparisons of different types of radiosondes already found that their humidity measurements have larger differences than temperature and pressure observations, Ferrare et al. (1995), Melfi et al. (1995) and

Wessel et al. (2000) also found these differences of water vapor profiles observed by their Raman lidar and radiosonde in the dry ambient air. Therefore, higher accuracy humidity sensors of radiosonde will improve the accuracy of calibrating water vapor Raman lidar. Meantime, the other calibrating method without radiosonde data has been considered (Evans et al. 2000). On the other hand, because tropospheric water vapor distributions show the quick temporal and spatial variations, the differences of measuring time and ambient air by Raman lidar and radiosonde also bring some discrepancies. L625 Raman lidar gives a one-hour mean of water vapor distribution in the vertical point of lidar, but GZZ-59 radiosonde gives a transient humidity at some altitude on its flying pathways.

Figure 3a illustrates the evolution of water vapor mixing ratio distribution with 2-hour long observations in the night of March 20, 2003. Gray colors represent the different values of water vapor mixing ratios. Every 8 minutes and 20 seconds, one profile of water vapor distribution is derived from L625 Raman lidar observations. We can see that water

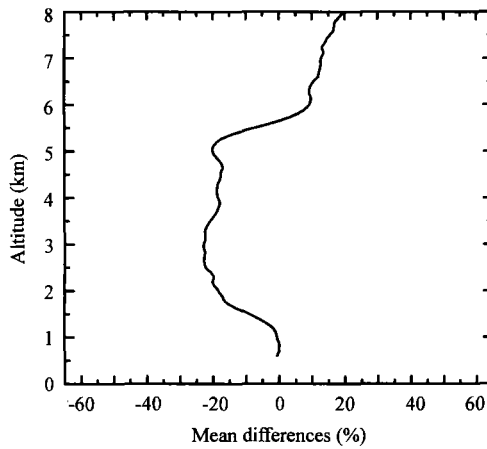


Fig. 2. Mean differences (%) of water vapor mixing ratios by 625 Raman lidar and GZZ-59 radiosonde ($(W_{\text{lidar}} - W_{\text{sonde}}) / W_{\text{lidar}}$).

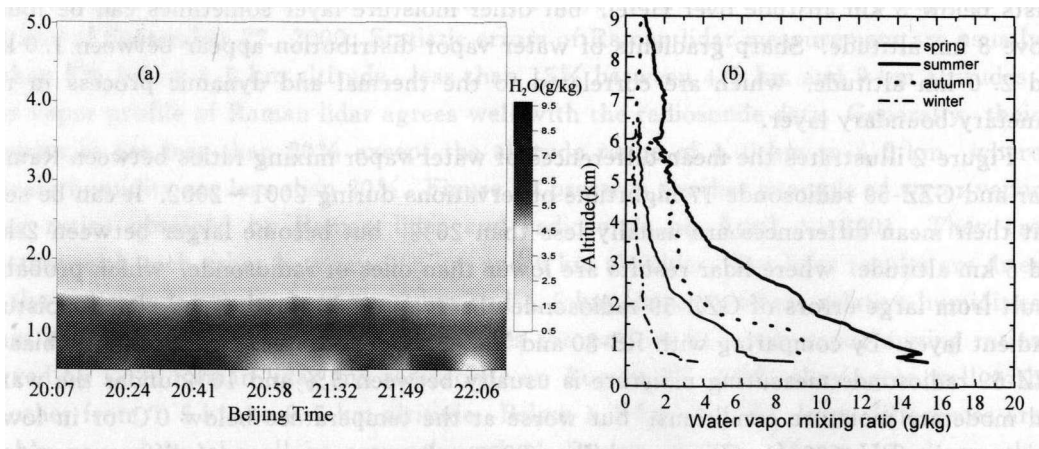


Fig. 3. (a) Temporal and (b) seasonal variations of water vapor mixing ratio distributions measured by Raman lidar.

vapor distributions were quite stable at that night, abundant water vapor appeared below 2 km altitude. Figure 3b presents the seasonal mean distributions of water vapor mixing ratios in the period of years 2001–2002. Significant seasonal variations of water vapor distribution are indicated. Water vapor mixing ratios are highest in summer until 8.5 km altitude, on the contrary, they are poorest in winter, which is mainly dominated by seasonal solar radiations and different flows in Hefei area. In summer, southeastern-flows from the Pacific Ocean to Hefei bring the rich water vapor. However, northwestern-winds dominate Hefei area with the cold and dry flow in the wintertime.

L625 Raman lidar can simultaneously measure tropospheric water vapor and aerosol distribution. Our observations frequently indicate that the distribution of aerosol optical parameters show good the correlation with water vapor mixing ratios distribution. As an example, Fig. 4 plots distributions of water vapor mixing ratios and aerosol scattering ratios at 355 nm obtained by L625 Raman lidar on the different days. Here, aerosol scattering ratio is defined as the ratio of total (aerosol plus molecule) backscattering to molecular backscattering coefficients. It is clear that similar structures of aerosol and water vapor mixing ratio appear below 3 km altitude. In Fig. 4b, similar structures appear between 3.5 km and 4.5 km altitudes, where maximum relative humidity is 51.2%, and Mie-scattering signals indicate that there were no clouds during lidar observations. Relative humidity is between 45% and 70% below 2 km in Fig. 4b and Fig. 4c.

Figure 5 images the time-height evolution of water vapor and aerosol scattering ratio distributions with about 1-hour long observations. Different gray colors represent the different values. It is much evident that high moisture and aerosol layers exist between 1.0 km and 2.2 km altitudes during lidar observations. Other Raman lidar also found these correlations between water vapor and aerosol optical properties in the free troposphere (Sakai et al. 1997). It can be understood that high moisture makes the hygroscopic aerosol particles grow, and refractive index of aerosol will be also changed, which probably result in aerosol optical properties changing (Hanel et al. 1981; Takamura et al. 1984). Influences of water vapor in aerosol optical properties are very interesting. Raman

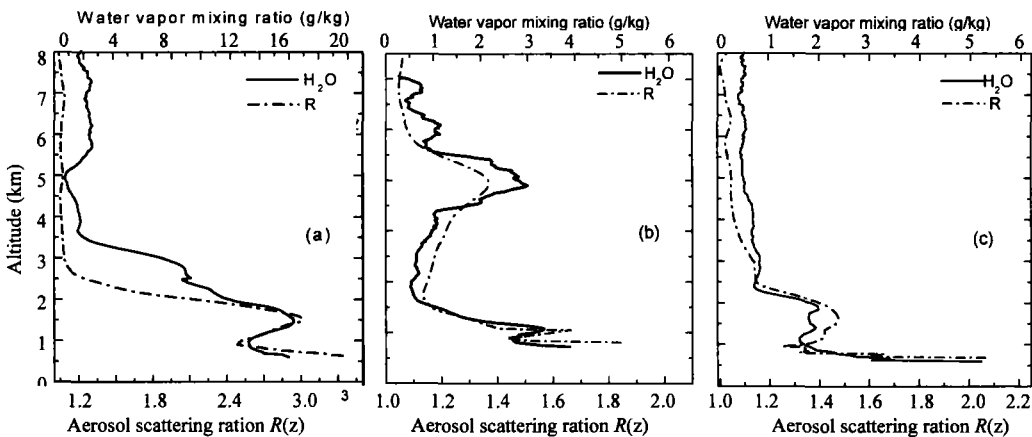


Fig. 4. Water vapor and aerosol scattering ratio distribution observed by Raman lidar over Hefei on (a) July 11, 2002, (b) January 23, and (c) December 9, 2002.

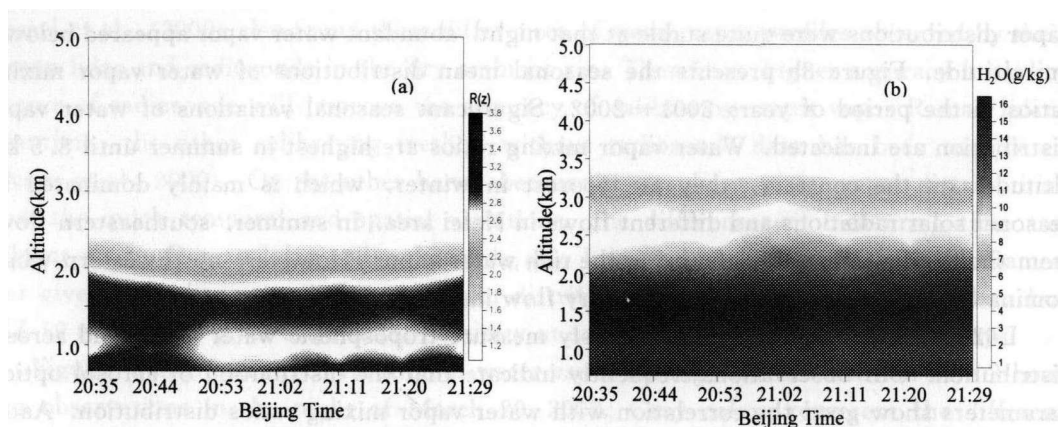


Fig. 5. Time-height images of (a) aerosol scattering ratio and (b) water vapor mixing ratio on July 11, 2002.

lidar measurements provide the unique opportunities for investigating these effects. Further observations and analysis are still needed for us.

IV. SUMMARY

This paper reports the Raman lidar for tropospheric water vapor measurements at Hefei, China. By comparing with GZZ-59 type radiosonde observations, their consistent results indicate that performances and measurements of this Raman lidar are reliable. Their mean differences of 17 nighttime observations are generally better than 20% under the moderate-high moisture conditions. Typical vertical profiles and general characteristics of water vapor distributions are presented. Seasonal variations of water vapor distribution are much significant over Hefei. Many measuring cases show the good correlation between aerosol optical properties and water vapor distribution in the lower troposphere. Further observations of this Raman lidar will contribute to analyze the statistic characteristics of water vapor distribution. High power Nd: YAG laser is highly expected to improve the temporal resolution and perform the daytime measurements of water vapor.

Acknowledgements: Mr. YUE Guming, Mr. Qli Fudi and Mr. XU Jisheng take part in building this Raman lidar. Mr. MA Chengsheng makes the measurements of radiosonde.

REFERENCES

- Evans, K. D., Demoz, B. B., Whiteman, D. N. et al. (2000), A new calibration technique for Raman lidar water vapor data. Proc. of. 20th International Laser Radar Conference, Vichy, France. 125–130.
- Ferrare, R. A., Melfi, S. H., Whiteman, D. N. et al. (1995), A comparison of water vapor measurements made by Raman lidar and radiosondes. *J. Atmos. Oceanic Technol.*, **23**: 1177–1195.
- Grant, W. B. (1991), Differential absorption and Raman lidar for water vapor profile measurements: a review. *Opt. Eng.*, **30**: 40–48.
- Hanel, Gottfried et al. (1981), Equilibrium size of aerosol particles and relative humidity: new experimental data from various aerosol types and their treatment for cloud physics applications. *Contrib. Atmos. Phy.*, **54**: 57–71.
- Li Tao, Qi Fudi, Jin Chuanjia et al. (2000), Raman lidar system for the measurement of water vapor

- mixing ratio in the atmosphere. *Chinese J. Atmos. Sci.*, **24**(6): 843–854 (in Chinese).
- Melfi, S. H., Whiteman, D., Ferrare, R. A. et al. (1995), Study of atmospheric water vapor using a Raman lidar, *Rev. Laser Eng.*, **23**(2), 105–111.
- Sakai, T., Shibata, T. and Iwasaka, Y. (1997), Relative humidity, backscattering ratio and depolarization as derived from Raman lidar observations, *J. Meteorol. Soc. Japan*, **75**: 1179–1185.
- Shine, K. P. and Sinda, A. (1991), Sensitivity of the earth's climate to height-dependent changes in water vapor mixing ration, *Nature*, **354**: 382–384.
- Takamura, T., Tanaka, M. and Nakajima, T. (1984), Effects of atmospheric humidity on the refractive index and the size distribution of aerosols as estimated from light scattering measurements, *J. Meteor. Soc. Japan*, **62** (3): 573–581.
- Turner, D. D., Feltz, W. F. and Ferrare, R. A. (2000), Continuous water vapor profiles from operational ground-based active and passive remote sensors, *Bull. Am. Meteor. Soc.*, **81**: 1301–1318.
- Wessel, J., M. Bech, Steven et al. (2000), Raman lidar calibration for the DMSP SSM/T-2 microwave water sensor, *IEEE Trans. Geosciences and Remote Sensing*, **38**: 141–153.
- Whiteman, D. N., Melfi, S. H., Ferrare, R. A. (1992), Raman lidar system for the measurements of water and aerosols in the earth's atmosphere, *Appl. Opt.*, **31**: 3068–3082.
- Whiteman, D. N., Murphy, W. F., Walsh, N. W. et al. (1993), Temperature sensitivity of an atmospheric Raman lidar system based on a XeF excimer laser. *Opt. Lett.*, **18**: 247–2498.
- Wu Yonghua, Hu Shunxing, Qi Fudi et al. (2002), Raman lidar measurements of aerosol and cloud optical properties in the troposphere. *Chinese J. Laser*, B11, 71–78.
- Zhang Aishen and Zhao Bolin Ed. (2000), *Modern Meteorological Observations*, Peking University Press, Beijing, 310–337 (in Chinese).